Available online at www.sciencedirect.com

ScienceDirect

Journal of the Franklin Institute 352 (2015) 686–707

Journal of The Franklin Institute

www.elsevier.com/locate/jfranklin

Estimation of lateral tire–road forces and sideslip angle for electric vehicles using interacting multiple model filter approach

XianJian Jin[a], Guodong Yin[a,b,*]

[a]School of Mechanical Engineering, Southeast University, Nanjing 211189, China
[b]State Key Laboratory of Mechanical Transmission, Chongqing University, Chongqing 400044, China

Received 30 December 2013; received in revised form 8 April 2014; accepted 21 May 2014
Available online 2 June 2014

Abstract

Vehicle control systems require certain vehicle information (e.g., tire–road forces and vehicle sideslip angle) concerning vehicle-dynamic parameters and vehicle–road interaction, which is difficult to measure directly for both technical and economedic reasons. This paper proposes a novel method to estimate lateral tire–road forces and vehicle sideslip angle by utilizing real-time measurements. The estimation method is based on an interacting multiple model (IMM) filter that integrates in-vehicle sensors of in-wheel-motor-driven electric vehicles to adapt multiple vehicle–road system models to variable driving conditions. Based on a four-wheel nonlinear vehicle dynamics model (NVDM) considering extended roll dynamics and load transfer, the vehicle–road system model set of the IMM filter is consists of a linear tire model based NVDM and a nonlinear Dugoff tire model based NVDM. Therefore, the IMM filter can integrate the estimates from two kinds of different vehicle–road system models to improve estimation accuracy. To address system nonlinearities and un-modeled dynamics, the interacting multiple model-unscented Kalman filter (IMM-UKF) and the interacting multiple model-extended Kalman filter (IMM-EKF) are investigated and compared simultaneously. Simulation using Matlab/Simulink-Carsim is carried out to verify the effectiveness of the proposed estimation methods. The results show that the developed estimation methods can accurately estimate lateral tire–road forces and the vehicle sideslip angle.

*Corresponding author at: School of Mechanical Engineering, Southeast University, Nanjing 211189, China. Tel.: +86 2552090501.
E-mail addresses: jinxianjian@yeah.net (X. Jin), ygd@seu.edu.cn (G. Yin).

http://dx.doi.org/10.1016/j.jfranklin.2014.05.008
0016-0032/

1. Introduction

Pure in-wheel-motor-driven electric vehicles (IWMD-EVs) have appeared as promising vehicle architectures based on several advantages in the viewpoint of high energy efficiency and advanced motion control. IWMD-EVs utilize in-wheel (or hub) motors to actuate the wheels respectively, and the torque of each wheel can be controlled independently. Such an actuation flexibility together with fast and accurate responses of the electric motors may improve the performance of advanced motion control systems [1,2]. Based on these advantages, a great deal of research on advanced motion systems, including direct yaw moment control system or electronic stability control system, has been done utilizing independently driven in-wheel motors in recent years [3,4,5].

However, performance and stability of vehicle motion control systems heavily depend on knowledge of important vehicle states. For instance, accurate knowledge of vehicle sideslip angle and tire–road forces means a better prediction of the real-time tire–road friction and the potential trajectories, which is very important for improving the management of vehicle motion control systems. Unfortunately, some fundamental data of advanced motion control systems (such as tire–road forces and vehicle sideslip angle) are difficult to measure in a standard car for both technical and economical reasons. As a consequence, tire–road forces and sideslip angle must be observed or estimated.

Lateral vehicle-dynamics estimation has been widely discussed in the literature. Several studies have been conducted concerning the estimation of tire–road forces and the vehicle sideslip angle. Vehicle-dynamics estimation based methods can be further classified into two categories. The first category is based linear vehicle model. Under normal driving conditions, the single track model "Bicycle model", which is linearized vehicle model and possesses sufficient accuracy, has been widely used to represent normal driving conditions for estimating vehicle states because the tire sideslip angle tends to be very small. Linear vehicle model based linear estimation methods were designed to estimate the sideslip angle, such as the Luenberger Observers, Recursive least squares algorithms and the Kalman filters. State observers derived from the Kalman filter were proposed and experimentally verified to estimate vehicle sideslip angle and other vehicle states using a linear vehicle model [6,7]. Novel estimation process of estimating vehicle sideslip and tire–road forces is divided into two blocks, the one is used to obtain tire–road forces utilizing a sliding-mode observer that is based on linear vehicle model, the other one that design the extended Kalman filter to estimate sideslip angle and cornering stiffness of tire [8].

However, under extreme driving maneuvers, linearized vehicle model based linear estimation methods have an inherent problem that cannot possess validity of tire due to the nonlinear dynamics of the tire's nature. If the vehicle undergoes high accelerations, the vehicle will have high slip angle and the vehicle's dynamic will become highly nonlinear simultaneously because of the nonlinear dynamics of the tire's inherent nature. The response of such a linear-vehicle-model-based method becomes less predictable, which means the behaviors of the vehicle will become uncontrollable and very dangerous in such situations. Compared to linear-vehicle-model-based methods, estimation methods based on nonlinear vehicle model is more close to real vehicle dynamics under extreme driving conditions. A great deal of research articles can be founded in order to deal with this problem of nonlinearities in the nonlinear vehicle model, a fuzzy observer that utilizes fuzzy model with T–S fuzzy rules to represent the nonlinear vehicle model was proposed to estimate vehicle slip angle [9]. Nonlinear techniques derived from extended Kalman filter and unscented Kalman filter were proposed, experimental results show a

low-cost method to estimate tire forces and sideslip angle, which have potential value for real applications [10,11]. Based on adaptation algorithm and lateral vehicle dynamics, an adaptive sideslip angle observer was designed [12,13]. A new estimation method was proposed by combining a dynamic and a kinematic vehicle model [14,15]. Novel estimation method that utilizes longitudinal difference between the left and right tire force for IWMD-EVs is proposed to estimate the tire cornering stiffness, experimental results also show this method provides good estimation against the variation of vehicle parameters [16]. Moreover, several researchers have proposed new estimation methods using new sensors. Estimation methods based on the extended Kalman filter and Bayesian selection were proposed to estimate nonlinear tire forces and road friction coefficient, the methods uses measures of the applied torques as inputs to vehicle model [17]. Based on sensors about lateral tire force, the extended Kalman filter and a RLS algorithm with a forgetting factor is used to estimate sideslip angle of IWMD-EVs by using measured lateral tire force [18]. A method was proposed to estimate vehicle sideslip angle, which is based on Global Positioning System (GPS) and inertial measurements without using the complex vehicle dynamics model [19,20,21]. Nevertheless, these new estimation methods require additional sensors (such as torques sensors, tire force sensors, GPS), and these additional sensors are often too expensive in practice, thus it is difficult for real applications of vehicle because of the additional sensor cost. In addition, GPS-based estimation methods may cause inaccurate estimation, especially for urban and forested driving conditions where visibility of satellite may be lost.

The modern passenger cars equipped with advanced motion control systems (AMCSs) already possess different types of vehicle motion sensors such as steering angle sensor, yaw rate and roll rate sensors, acceleration sensors, and wheel speed sensors [22,23,24], thus the fusion of data from different types of sensors becomes very important for improving performance of AMCSs. The performance of AMCSs depends not only on the filter structure but also on the appropriate choice of vehicle model. The importance about the roles for different types of vehicle models in advanced motion control systems were investigated in [25,26], the results show that a appropriate vehicle model provides significantly better performance for advanced motion control systems compared with a poor vehicle model by using the same algorithm. While, in practice, choosing an optimal model is very difficult for variable driving conditions, the multiple model (MM) approach utilizes a set of models to represent possible vehicle model due to different driving conditions, which can obtained more accurate vehicle states by combining filters based on corresponding vehicle model of a finite number of different models compared with single vehicle model. Among several MM estimation approaches, the interacting MM (IMM) filter that possesses high accurate and low computational load has become the most popular [27].

This paper presents an IMM filter-based vehicle states estimation methods that consider the changing of driving conditions in which a vehicle can be operated. To adaptively adjust to adapt change vehicle dynamic characteristics and to compare system nonlinearities under diversified driving conditions, the vehicle–road system model set based on the IMM filter is consists of a linear tire model based NVDM and a nonlinear Dugoff tire model based NVDM. The linear tire model based NVDM and the nonlinear Dugoff tire model based NVDM are both appropriate for small slip angle driving conditions such as under normal driving conditions (small accelerations). Under extreme driving maneuvers (high accelerations), only the nonlinear Dugoff tire model based NVDM is suitable for such as large sideslip angle driving conditions. The IMM filter based vehicle states estimation methods weights the suitable vehicle model to match the corresponding driving condition through the stochastic process, which can provide more accurate estimation of vehicle states as compared to the single model filter for diversified driving conditions. The overall architecture of the IMM filter based estimation system is described in Fig. 1.

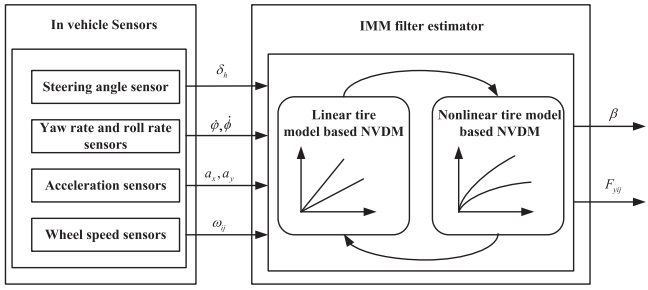

Fig. 1. The overall architecture of the IMM filter based estimation system.

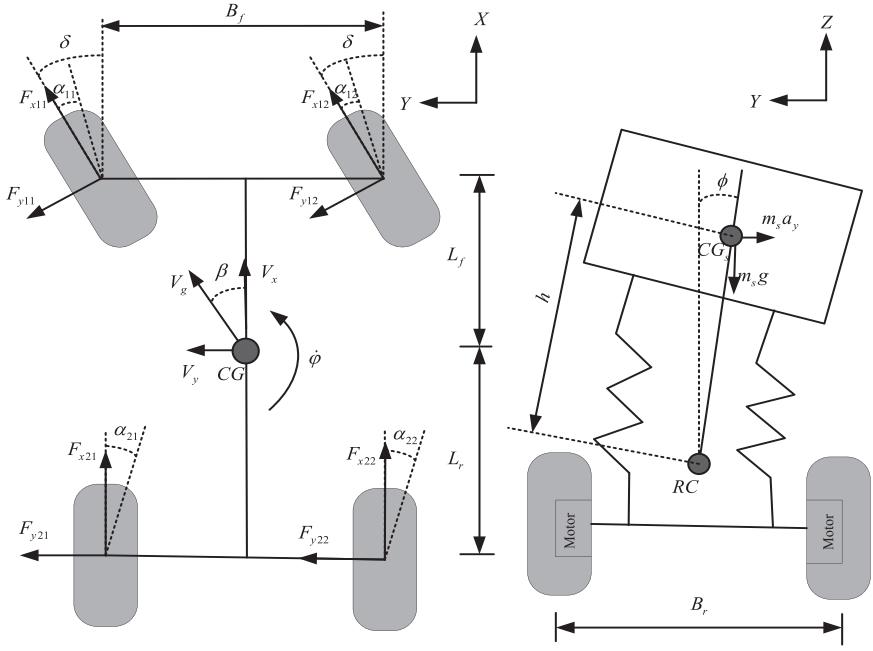

Fig. 2. Four-wheel nonlinear vehicle dynamics model.

The remainder of the paper is organized as follows. Section 2 presents the vehicle–road system model set. In Section 3, estimation methods of interacting multiple model filter are design. In Section 4, simulation results are presented and discussed. Finally, conclusions are offered in Section 5.

2. Vehicle–road system model set

2.1. Four-wheel nonlinear vehicle dynamics model

Fig. 2 shows the vehicle dynamics model for electric vehicles with in-wheel motors. Four-wheel nonlinear vehicle dynamics model chosen in this study consists of an eight-degree-of-freedom (8-DOF) model, which includes longitudinal and lateral motions, yaw and roll motion of

the vehicle, and the rotational dynamics of the four wheels, is widely used to describe behavior of lateral vehicle dynamic [17,25]. The 8-DOF vehicle dynamic motion are therefore derived as Eqs. (1)–(4), which represent the longitudinal, lateral, yaw, and roll dynamics, respectively.

$$m(\dot{V}_x - V_y\dot{\varphi}) + m_s h\dot{\varphi}\dot{\phi} = \sum_{i,j=1}^{2} F_{xij} = (F_{x11}+F_{x12})\cos\delta + (F_{x21}+F_{x22}) - (F_{x11}+F_{x12})\sin\delta = ma_x \tag{1a}$$

$$m(\dot{V}_y + V_x\dot{\varphi}) - m_s h\ddot{\phi} = \sum_{i,j=1}^{2} F_{yij} = (F_{y11}+F_{y12})\cos\delta + (F_{y21}+F_{y22}) - (F_{y11}+F_{y12})\sin\delta = ma_y \tag{1b}$$

$$m\dot{V}_g = (F_{x11}+F_{x12})\cos(\beta-\delta) + (F_{x21}+F_{x22})\cos\beta + m_s h\ddot{\phi}\sin\beta + (F_{y11}+F_{y12})sin(\beta-\delta) + (F_{y21}+F_{y22})\sin\beta - m_s h\dot{\varphi}\dot{\phi}\cos\beta \tag{2a}$$

$$m(\dot{\beta}+\dot{\varphi})V_g = (F_{y11}+F_{y12})cos(\beta-\delta) + (F_{y11}+F_{y12})cos\beta - m_s h\dot{\varphi}\dot{\phi}\sin\beta - (F_{x11}+F_{x12})\sin(\beta-\delta) - (F_{x11}+F_{x12})\sin\beta + m_s h\ddot{\phi}\cos\beta \tag{2b}$$

$$I_{zz}\ddot{\varphi} - I_{xz}\ddot{\phi} = \sum M_z \tag{3a}$$

$$\sum M_z = (F_{y11}\sin\delta - F_{x11}\cos\delta)\frac{B_f}{2} - (F_{x11}\sin\delta + F_{y11}\cos\delta)L_f + (F_{x12}\cos\delta - F_{y12}\sin\delta)\frac{B_f}{2} - (F_{x12}\sin\delta + F_{y12}\cos\delta)L_f + (F_{x22}-F_{x21})\frac{B_r}{2} + (F_{y22}+F_{y21})L_r \tag{3b}$$

$$I_{xxs}\ddot{\varphi} - I_{xzs}\ddot{\phi} = \sum M_x \tag{4a}$$

$$\sum M_x = m_s h(V_y + V_x\dot{\varphi}) + m_s hg\phi - (C_{\phi f}+C_{\phi r})\dot{\phi} - (K_{\phi f}+K_{\phi r})\phi \tag{4b}$$

where $\sum_{i,j=1}^{2} F_{xij}$, $\sum_{i,j=1}^{2} F_{yij}$ are the sum of the longitudinal and lateral forces on the four tires, respectively. $\sum M_z$, $\sum M_x$ are total yaw moments and total roll moments, respectively. V_x, V_y are vehicle longitudinal velocity at center of gravity (CG) and vehicle lateral vehicle velocity at CG, respectively. φ, ϕ and β are yaw angle, the roll angle and the vehicle side slip angle respectively. δ is the front steering angle, the front steering angles on left and right wheel are assumed to be equal ($\delta_{11}=\delta_{12}=\delta$). m, m_s and h are the total mass, the sprung mass, the distances from roll axis to the CG of sprung mass respectively, F_{xij} and F_{yij} are the longitudinal tire force and lateral tire force of the i, jth wheel, respectively, i stands for left or front, j stands for right or rear. I_{zz}, I_{xz}, I_{xxs} and I_{xzs} are vehicle moment of inertia about yaw axes, vehicle product of inertia bout roll and yaw axes, sprung mass product of inertia about roll and yaw axes and sprung mass moment of inertia about roll axes respectively, B_f, B_r, L_f and L_r are front track width, rear track width, the distances from the CG to the front and rear axle respectively, $K_{\phi f}$ and $K_{\phi r}$ are the front and rear roll stiffness, respectively. $C_{\phi f}$ and $C_{\phi r}$ are the front and rear roll damping coefficient, respectively.

In contrast to conventional vehicles, IWMD-EVs that have battery packs under the floor and driving motors attached in wheels, the tires have more unsprung mass, and effects of load

transfer for tire with in-wheel motor are critical. Therefore, effects of load transfer for variations on tire forces cannot be neglected, and then the tire normal force considering the load transfers due to longitudinal and lateral accelerations can be described as:

$$F_{z11} = \frac{mgL_f}{2L} - \frac{mh_{cg}a_x}{2L} - \frac{a_y}{B_f}\left(\frac{m_s h_{rf} L_{rs}}{L} + m_{usf} h_{uf}\right) - \frac{1}{B_f}(-K_{\phi f}\phi - C_{\phi f}\dot{\phi}) \tag{5a}$$

$$F_{z12} = \frac{mgL_f}{2L} - \frac{mh_{cg}a_x}{2L} + \frac{a_y}{B_f}\left(\frac{m_s h_{rf} L_{rs}}{L} + m_{usf} h_{uf}\right) + \frac{1}{B_f}(-K_{\phi f}\phi - C_{\phi f}\dot{\phi}) \tag{5b}$$

$$F_{z21} = \frac{mgL_f}{2L} + \frac{mh_{cg}a_x}{2L} - \frac{a_y}{B_r}\left(\frac{m_s h_{rr} L_{fs}}{L} + m_{usr} h_{ur}\right) - \frac{1}{B_r}(-K_{\phi r}\phi - C_{\phi r}\dot{\phi}) \tag{5c}$$

$$F_{z22} = \frac{mgL_f}{2L} + \frac{mh_{cg}a_x}{2L} + \frac{a_y}{B_r}\left(\frac{m_s h_{rr} L_{fs}}{L} + m_{usr} h_{ur}\right) + \frac{1}{B_r}(-K_{\phi r}\phi - C_{\phi r}\dot{\phi}) \tag{5d}$$

where a_x and a_y are longitudinal and lateral acceleration, respectively. m_{usf}, m_{usr} and h_{cg} are front unsprung mass, rear unsprung mass and height of center of gravity respectively. h_{rf} and h_{rr} are height of the front roll center and height of the rear roll center, respectively. h_{uf} and h_{ur} heights of the front and rear unsprung mass CG, respectively. L_{fs} and L_{rs} are distances from the CG of the sprung mass to the front and rear axles, respectively.

2.2. Linear and nonlinear tire model

2.2.1. Tire nonlinearity

Since the quality of the estimation method largely depends on the accuracy of the tire model, the applied model must be precise. Based on the specifications of the experimental electric vehicle in our laboratory (Fig. 3), the features of the tire model are obtained. Table 1 presents the specifications of experimental electric vehicle.

Fig. 4 describes the lateral tire force versus the tire slip angle, the importance of tire nonlinearity in the tire model can be observed in Fig. 4. At small tire slip angle, the lateral tire force of the linear model has the nearly same level as that of the nonlinear model. It is appropriate for small tire slip angles to define the force profile by using a linear region. Under normal driving conditions, the vehicle accelerations tend to small, the tire operates in this linear region. When

Fig. 3. The experimental electric vehicle.

Table 1
The specifications of experimental electric vehicle.

Parameter	Value
Sprung mass	1125 kg
Front and rear unsprung mass, m_{usf}, m_{usr}	82.5, 95.8 kg
Distance, the CG to front and rear axle, L_f, L_r	1.1, 1.3 m
Vehicle moment of inertia about yaw axis, I_{zz}	1519 kg m^2
Front and rear track width, B_f, B_r	1.38, 1.35 m
Vehicle product of inertia about roll and yaw axes, I_{xz}	50.2 kg m^2
Distance, roll axis to sprung mass, h	0.174 m
Wheel moment of inertia, I_w	1.28 kg m^2
Wheel radius, R_w	0.272 m
Sprung mass moment of inertia about roll axis, I_{xxs}	325 kg m^2
Front and rear roll center height, h_{rf}, h_{rr}	0.205, 0.013 m
Sprung mass product of inertia about roll and yaw axes, I_{xzs}	10.6 kg m^2
Front and rear roll steer coefficient,ε_f, ε_r	0.065, 0.012 rad/rad
Front and rear cornering stiffness, C_{yf}, C_{yr}	15,325, 16,280 N/rad

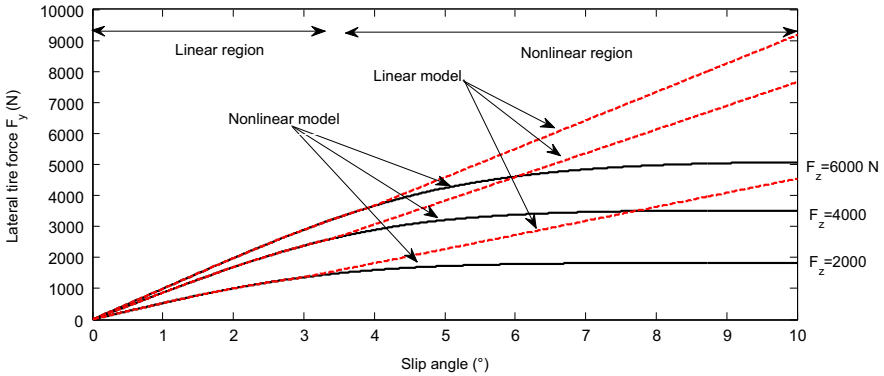

Fig. 4. The lateral tire force versus the tire slip angle.

the tire slip angle continues to grow, the lateral tire force of the linear model has a distinct difference than that of the nonlinear model, and then the lateral tire force becomes nonlinear. Under extreme driving maneuvers, the vehicle undergoes high accelerations, the vehicle will have high slip angle and the vehicle's dynamic will become highly nonlinear simultaneously because of the nonlinear dynamics of the tire's inherent nature. If the lateral tire force in this nonlinear region is treated as linear, the behaviors of the vehicle will become uncontrollable and very dangerous in such nonlinear situations. Therefore, building precise nonlinear tire model is essential for improving quality of the estimation under extreme driving maneuvers.

Under extreme driving maneuvers, lateral and longitudinal tire–road forces are a function of the tire properties (including material, tread pattern, and pressure), the normal load on the tire, and the other factors of tire. The relation between these factors is extremely complex and nonlinear.

However, taking into account real-time implementation requirement, the tire model should be also precise and simple simultaneously, as computational effort of control algorithm relates to algorithm execution time. Due to often limited system computational resources and the need to make fast decision of vehicle control systems, the computational effort is very critical for real applications of vehicle control systems. The tire forces are inherently coupled under extreme

driving maneuvers, the coupling between longitudinal tire force and lateral tire force cannot be coupled in nonlinear region, however, under normal driving conditions, and the tire operates in linear region, the nonlinear constraints of tire forces can be decoupled into independent linear constraints, and precision of the linear tire model is sufficient. As can be seen from two tire models, the linear tire model is much simpler than the nonlinear tire model. If the estimation algorithm often uses the nonlinear tire model in most cases (under normal driving conditions), it will inordinately enhance the computational load and affect the fast response of vehicle control systems. Hence, the nonlinear tire model is not suitable to take the place of linear tire model under normal driving conditions.

Besides, if the estimation algorithm makes use of a single Kalman filter, the transition between linear and nonlinear mode will cause a serious measurement error for estimating the lateral tire–road forces and the vehicle sideslip angle. Because the estimated covariance matrices of the measurement noise by the corresponding Kalman filter are not adaptively adjusted to match the true covariance variation between the linear and nonlinear cases. But the IMM estimation algorithm has recently been demonstrated as a self-adjusting variable-bandwidth filter that makes it suitable for hybrid dynamic systems with switching-mode [28,29].

Therefore, using interacting multiple model filter is essential for improving quality of the estimation, which is adaptively adjusted to adapt variable driving conditions.

2.2.2. *Linear tire model*

At small slip angles, the tire operates in this linear region, the accuracy of the linear tire model is appropriate. To compared linearity and nonlinearities of tire model under various driving conditions, a simple tire model is built. According to [9,12], from the linear model, the tire slip angles can be expressed as the following:

$$\begin{bmatrix}\alpha_{11}\\ \alpha_{12}\\ \alpha_{21}\\ \alpha_{22}\end{bmatrix}=\begin{bmatrix}\delta\\ \delta\\ 0\\ 0\end{bmatrix}-\begin{bmatrix}\xi_{11}\\ \xi_{12}\\ \xi_{21}\\ \xi_{22}\end{bmatrix} \tag{6}$$

For small angles, ξ_{ij} can be explicitly written as

$$\begin{bmatrix}\xi_{11}\\ \xi_{12}\\ \xi_{21}\\ \xi_{22}\end{bmatrix}=\tan^{-1}\begin{bmatrix}\frac{V_y+L_f\dot{\varphi}}{V_x-B_f\dot{\varphi}/2}\\ \frac{V_y+L_f\dot{\varphi}}{V_x+B_f\dot{\varphi}/2}\\ \frac{V_y-L_r\dot{\varphi}}{V_x-B_r\dot{\varphi}/2}\\ \frac{V_y-L_r\dot{\varphi}}{V_x+B_r\dot{\varphi}/2}\end{bmatrix}\approx\begin{bmatrix}\frac{V_y+L_f\dot{\varphi}}{V_x-B_f\dot{\varphi}/2}\\ \frac{V_y+L_f\dot{\varphi}}{V_x+B_f\dot{\varphi}/2}\\ \frac{V_y-L_r\dot{\varphi}}{V_x-B_r\dot{\varphi}/2}\\ \frac{V_y-L_r\dot{\varphi}}{V_x+B_r\dot{\varphi}/2}\end{bmatrix}$$

Considering the roll angle effects in Eq. (6), the tire slip angles can be written as

$$\begin{bmatrix}\alpha_{11}\\ \alpha_{12}\\ \alpha_{21}\\ \alpha_{22}\end{bmatrix}=\begin{bmatrix}\delta\\ \delta\\ 0\\ 0\end{bmatrix}+\begin{bmatrix}\varepsilon_f\\ \varepsilon_f\\ \varepsilon_r\\ \varepsilon_r\end{bmatrix}\phi-\begin{bmatrix}\frac{V_y+L_f\dot{\varphi}}{V_x-B_f\dot{\varphi}/2}\\ \frac{V_y+L_f\dot{\varphi}}{V_x+B_f\dot{\varphi}/2}\\ \frac{V_y-L_r\dot{\varphi}}{V_x-B_r\dot{\varphi}/2}\\ \frac{V_y-L_r\dot{\varphi}}{V_x+B_r\dot{\varphi}/2}\end{bmatrix} \tag{7}$$

When the tire operates in linear region, the lateral and longitudinal tire forces can be linearly approximated as follows:

$$F_{yij} = -C_{yij}\alpha_{ij} \tag{8a}$$

$$F_{xij} = k_\mu \lambda_{ij} F_{zij} \tag{8b}$$

where C_{yij} is cornering stiffness of each tire, k_μ is a slope about μ–λ_{ij} curve in the linear region.

2.2.3. Nonlinear Dugoff tire model

The most commonly used nonlinear models include Dugoff and Pacejka tire models. The Pacejka tire model "Magic Formula" requires a large number of tire-specific parameters that are usually unknown. For this reason, Dugoff nonlinear tire model is selected here. Compared to Pacejka model, the Dugoff nonlinear tire model synthesizes the tire property into the parameters C_x and C_y [30], which referred to as the longitudinal and the lateral cornering stiffness of the tire. Tire slip angles can be written as

$$\begin{bmatrix}\alpha_{11}\\ \alpha_{12}\\ \alpha_{21}\\ \alpha_{22}\end{bmatrix} = \begin{bmatrix}\delta\\ \delta\\ 0\\ 0\end{bmatrix} + \begin{bmatrix}\varepsilon_f\\ \varepsilon_f\\ \varepsilon_r\\ \varepsilon_r\end{bmatrix}\phi - \tan^{-1}\begin{bmatrix}\frac{V_y+L_f\dot{\varphi}}{V_x-B_f\dot{\varphi}/2}\\ \frac{V_y+L_f\dot{\varphi}}{V_x+B_f\dot{\varphi}/2}\\ \frac{V_y-L_r\dot{\varphi}}{V_x-B_r\dot{\varphi}/2}\\ \frac{V_y-L_r\dot{\varphi}}{V_x+B_r\dot{\varphi}/2}\end{bmatrix} \tag{9}$$

Lateral and longitudinal tire–road forces can be defined as follows:

$$F_{yij} = \frac{C_{yij}\ \tan\ \alpha_{ij}}{1-\lambda_{ij}} f(S) \tag{10a}$$

$$\begin{aligned} F_{xij} &= \tfrac{C_{xij}\lambda_{ij}}{1-\lambda_{ij}} f(S)\\ S &= \frac{\mu F_{zij}(1-\varepsilon_r V_x\sqrt{\lambda_{ij}^2+\tan^2\alpha_{ij}})}{2\sqrt{C_{ij}^2\lambda_{ij}^2+C_{ij}^2\tan^2\alpha_{ij}}}(1-\lambda_{ij}^2)\\ f(S) &= \begin{cases}1 & S>1\\ S(2-S) & S<1\end{cases} \lambda_{ij} = \tfrac{R_w\omega_{ij}-V_x}{\max(R_w\omega_{ij},V_x)} \end{aligned} \tag{10b}$$

where ε_f and ε_r are front and rear roll steer coefficient, respectively.

2.2.4. Time lag of the tire model

When the sideslip angle changes, a lateral tire force is created with a time lag. According to [29], a relaxation length can be used to describe this transient behavior of tires. The tire–road forces can be written as follows:

$$\dot{F}_{yij} = \frac{V_g}{\sigma_{ij}}(-F_{yij} + \overline{F}_{yij}) \tag{11a}$$

$$\dot{F}_{xij} = \frac{V_g}{\sigma_{ij}}(-F_{xij} + \overline{F}_{xij}) \tag{11b}$$

where $\overline{F}_{yij}$ and $\overline{F}_{xij}$ are the quasi-static Dugoff tire-force, σ_{ij} is the relaxation length, which is the distance covered by the tire while the tire force is kicking in.

3. Interacting multiple model filter estimator

The overall process of proposed IMM-based estimation system is shown in Fig. 5. The proposed estimation method estimate the model probabilities and weighs the appropriate vehicle model to adapt to changing driving conditions by making use of the stochastic processes, and then, integrates the estimates of each model to improve estimation accuracy. Under normal driving conditions, the tire operates in this linear region, the linear tire model based NVDM and the nonlinear Dugoff tire model based NVDM are both appropriate. However, under extreme driving maneuvers, the behavior of the tire presents nonlinear feature, only the nonlinear Dugoff tire model based NVDM is suitable because it considers nonlinearity of the tire. Although the EKF is widely used to estimate states of nonlinear dynamics systems, linearization errors of the EKF are significant because the EKF uses Jacobian matrices to linearly approximate nonlinear system with first-order linearization. In contrast to the EKF algorithm, UKF utilizes a set of sigma points to realize nonlinear transformation, which acts directly on the nonlinear dynamics systems in order to approximate the states, thus the significant linearization errors of EKF can be avoided. UKF has proved to be a powerful nonlinear estimation technique, especially for strong nonlinearities systems [27]. When the tire enters a nonlinear region, the vehicle–road system presents strong nonlinearities. For these reasons, UKF is selected in this study, and EKF is used to compare. For further information concerning IMM-EKF, refer to [31]. The IMM-UKF estimator is divided into four parts: interacting, filtering, model probability updating, and estimation fusion.

3.1. Interacting

Initially, the multiple-mode states from estimation of the previous step are combined with the mixing weight at this mixed stage. The mixing weight can be expressed as:

$$\mu_{j|i,k-1|k-1} = \frac{1}{\overline{c}_{i,k|k-1}} p_{ji}\mu_{j,k-1} \tag{12a}$$

where $\mu_{j,k-1}$ is the model probability of model j in the previous step. The mixing probabilities

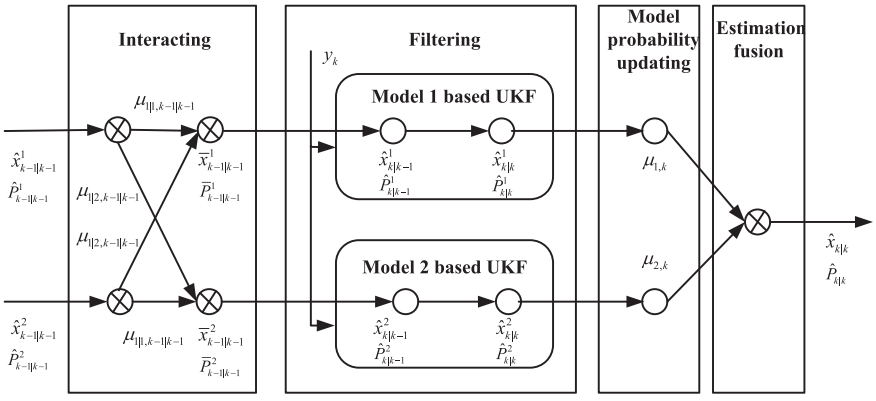

Fig. 5. Process of the IMM-UKF.

are written as

$$\overline{c}_{i,k|k-1} = \sum_{j=1}^{2} p_{ji}\mu_{j,k-1} \tag{12b}$$

The model transition of the IMM filter between models is subject to the Markov process with prior information, which is characterized by the transition probability matrix p_{ji}. The model transition probability matrix p_{ji} describes the probability that the vehicle model will make a transition from model j to model i. The transition probability matrix p_{ji} can be described as

$$p_{ij} = \begin{bmatrix} 0.98 & 0.02 \\ 0.01 & 0.99 \end{bmatrix} \tag{13}$$

where $i, j = 1, 2$ represent the linear tire model based NVDM and nonlinear Dugoff tire model based NVDM, respectively. These values of the transition probability matrix were calculated using a statistical method, which related to the sojourn times and sampling interval of the real driving condition in the real engineering problem, this choice depends on the fact that the linear or the nonlinear mode of each tire is changed for each 200 samples under the linear/the nonlinear mode of transition cases, and at the start the two models have the same chance to be selected for the real applications [32,33,34,35].

The mixed a priori state estimation and covariance of model i are

$$\overline{x}^{i}_{k-1|k-1} = \sum_{j=1}^{2} \hat{x}^{j}_{k-1|k-1}\mu_{j|i,k-1|k-1} \tag{14a}$$

$$\overline{P}^{i}_{k-1|k-1} = \sum_{j=1}^{2} \mu_{j|i,k-1|k-1}\left[\hat{P}^{j}_{k-1|k-1} + (\hat{x}^{j}_{k-1|k-1} - \overline{x}^{i}_{k-1|k-1})(\hat{x}^{j}_{k-1|k-1} - \overline{x}^{i}_{k-1|k-1})^{T}\right] \tag{14b}$$

where $\hat{P}^{j}_{k-1|k-1}$ and $\hat{x}^{j}_{k-1|k-1}$ are the state estimation and covariance of model j in the previous step, respectively.

3.2. Model-matched filtering

Fig. 6 presents the UKF architecture for model i. Using the initial mixing state and the covariance of the interacting step, the UKF of each model predicts and updates the model state and covariance. The nonlinear state-space representation of linear tire model based NVDM and the nonlinear Dugoff tire model based NVDM can be described as follows:

$$\begin{aligned} \dot{x}_{(t)} &= f(x_{(t)}, u_{(t)}) + \omega_{(t)} \\ y(t) &= h(x_{(t)}, u_{(t)}) + v_{(t)} \end{aligned} \tag{15}$$

The input vector u includes wheel speed of each wheel and the steering wheel angle (see Fig. 1).

$$u = [\delta_h, \omega_{11}, \omega_{12}, \omega_{21}, \omega_{22}] \tag{16}$$

The measure vector y includes roll rate, yaw rate, wheel speed, longitudinal, and lateral accelerations.

$$y = [a_x, a_y, \dot{\varphi}, \dot{\phi}, \omega_{11}, \omega_{12}, \omega_{21}, \omega_{22}] \tag{17}$$

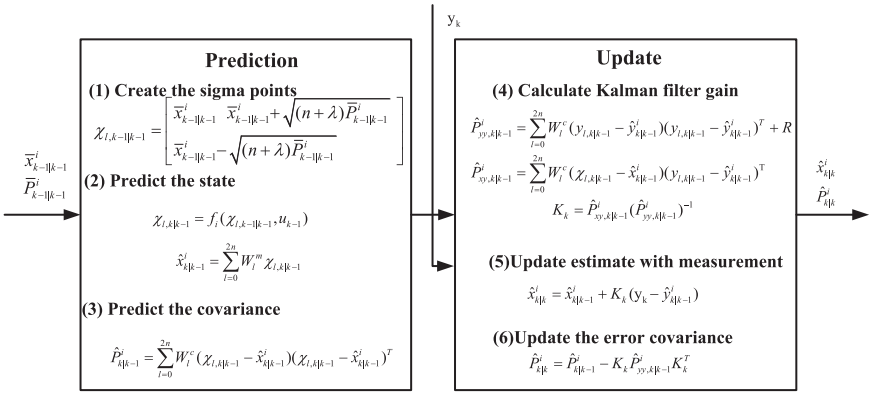

Fig. 6. UKF for each single model filter.

The state vector x includes roll rate, yaw rate, roll angle, vehicle velocity, sideslip angle at the CG, lateral tire–road forces, and longitudinal tire–road forces.

$$x=[\dot{\varphi},\dot{\phi},\phi,V_g,\beta,F_{y11},F_{y12},F_{y21},F_{y22},F_{x11},F_{x12},F_{x21},F_{x22}] \tag{18}$$

where w and v are the process and measurements noise vectors, respectively, are assumed to be white, zero mean, and uncorrelated.

Therefore, the particular nonlinear function f (.) of the state Eq. (19) is derived as follows:

$$\begin{cases} f_1=\frac{1}{I_{zz}[(I_{xxs}-m_sh)I_{zz}-I_{xzs}I_{xz}]}\begin{bmatrix}(I_{xxs}-m_sh)[(x_6\ \sin\ u_1-x_{10}\ \cos\ u_1+x_{11}\ \cos\ u-x_7\ \sin\ u_1)B_f/2\\ -(x_{10}\ \sin\ u_1+x_6\ \cos\ u_1+x_{11}\ \sin\ u_1+x_7\ \cos\ u)L_f+(x_{13}-x_{12})\\ B_r/2+(x_9+x_8)L_r]+I_{xzs}I_{xz}[(x_6+x_7)cosu_1-(x_6+x_7)\sin\ u_1\\ +x_8+x_9+m_shgx_3-(C_{\phi f}+C_{\phi r})x_2-(K_{\phi f}-K_{\phi r})x_3]\end{bmatrix}\\ f_2=\frac{1}{(I_{xxs}-m_sh)I_{zz}-I_{xzs}I_{xz}}\begin{bmatrix}I_{xzs}[(x_6\ \sin\ u_1-x_{10}\ \cos\ u_1+x_{11}\ \cos\ u-x_7\ \sin\ u_1)B_f/2-(x_{10}\ \sin\ u_1\\ +x_6\ \cos\ u_1+x_{11}\ \sin\ u_1+x_7\ \cos\ u)L_f+(x_{13}-x_{12})B_r/2+(x_9+x_8)\\ L_r]+I_{zz}[(x_6+x_7)\cos\ u_1-(x_6+x_7)\sin\ u_1+x_8+x_9+m_shgx_3\\ -(C_{\phi f}+C_{\phi r})x_2-(K_{\phi f}-K_{\phi r})x_3]\end{bmatrix}\\ f_3=x_2\\ f_4=\frac{1}{m}\begin{bmatrix}(x_{10}+x_{11})cos(x_5-u_1)+(x_{12}+x_{13})cosx_5+(x_6+x_7)\sin(x_5-u_1)-m_shx_1x_2\ \cos\ x_5\\ +(x_8+x_9)\sin\ x_5+m_shf_2\ \sin\ x_5\end{bmatrix}\\ f_5=\frac{1}{mx_4}\begin{bmatrix}(x_6+x_7)cos(x_5-u_1)+(x_8+x_9)cosx_5-(x_{10}+x_{11})\sin(x_5-u_1)-m_shx_1x_2\ \sin\ x_5\\ -(x_{12}+x_{13})\sin\ x_5+m_shf_2\ \cos\ x_5\end{bmatrix}-x_1\\ f_6=\frac{x_4}{\sigma_{11}}(-x_6+\overline{F}_{y11}),\ f_7=\frac{x_4}{\sigma_{12}}(-x_7+\overline{F}_{y12}),\ f_8=\frac{x_4}{\sigma_{21}}(-x_8+\overline{F}_{y21}),\ f_9=\frac{x_4}{\sigma_{22}}(-x_9+\overline{F}_{y22})\\ f_{10}=\frac{x_4}{\sigma_{11}}(-x_{10}+\overline{F}_{x11}),\ f_{11}=\frac{x_4}{\sigma_{12}}(-x_{11}+\overline{F}_{x12}),\ f_{12}=\frac{x_4}{\sigma_{21}}(-x_{12}+\overline{F}_{x21}),\ f_{13}=\frac{x_4}{\sigma_{22}}(-x_{13}+\overline{F}_{x22})\end{cases} \tag{19}$$

The particular observation h(.) is derived as follows

$$\begin{cases} h_1=\frac{1}{m}[(x_{10}+x_{11})cosu_1-(x_{10}+x_{11})\sin\ u_1+x_{12}+x_{13}]\\ h_2=\frac{1}{m}[(x_6+x_7)cosu_1-(x_6+x_7)\sin\ u_1+x_8+x_9]\\ h_2=x_3,\ h_4=x_4,\ h_5=x_5,\ h_6=x_6,\ h_7=x_7,\ h_8=x_8\end{cases} \tag{20}$$

Using above mentioned equations, applying the IMM-UKF can estimate the state vector $x_{(t)}$.

1) *Create the sigma points*. In order to approximate the vehicle states, UKF utilizes a nonlinear transformation (unscented transformation) that uses a set of carefully chosen sigma points to act on the true nonlinear dynamics systems. The set of $2n+1$ sigma points can be created:

$$\chi_{l,k-1|k-1} = \left[\overline{x}^i_{k-1|k-1} \quad \overline{x}^i_{k-1|k-1} + \sqrt{(n+\lambda)\overline{P}^i_{k-1|k-1}} \quad \overline{x}^i_{k-1|k-1} - \sqrt{(n+\lambda)\overline{P}^i_{k-1|k-1}}\right] \tag{21a}$$

$$\begin{aligned}
&\chi_{0,k-1|k-1} = \overline{x}^i_{k-1|k-1}\\
&\chi_{l,k-1|k-1} = \overline{x}^i_{k-1|k-1} + \sqrt{(n+\lambda)\overline{P}^i_{k-1|k-1}}, l = 1,\ 2, \ldots,\ n\\
&\chi_{l,k-1|k-1} = \overline{x}^i_{k-1|k-1} - \sqrt{(n+\lambda)\overline{P}^i_{k-1|k-1}}, l = n+1,\ n+2, \ldots,\ 2n
\end{aligned} \tag{21b}$$

and the associated weights:

$$\begin{aligned}
&W^m_0 = \kappa/(n+\kappa)\\
&W^c_0 = \kappa/(n+\kappa) + (1-\alpha^2+\beta_t)\\
&W^m_l = 1/2(n+\kappa),\ l = 1,\ 2, \ldots,\ 2n\\
&W^c_l = 1/2(n+\kappa),\ l = 1,\ 2, \ldots,\ 2n
\end{aligned} \tag{21c}$$

$$\kappa = \alpha^2(n+s) - n \tag{22}$$

where α, β_t and s are influencing factor about the unscented transformation. The parameter α that is used to describe the transformational spread of the sigma points is usually set 1e-$4 \le \alpha \le 1$, this study choose α equal 0.5. The constant β_t that is related to the prior knowledge of the distribution of x, and choosing $\beta_t = 2$ is optimal under the Gaussian distributions. The s is usually set to 0.

2) *Prediction with the process model*. In this step, the predicted state $\hat{x}^i_{k|k-1}$ and its covariance $\hat{P}^i_{k|k-1}$ are obtained. The state vector is augmented with the process and noise terms to give an $n = n+q$ dimensional vector $x_{k-1} = [x_{k-1}\ \omega_{k-1}]$. The transformed set can be written as

$$\chi_{l,k|k-1} = f_i(\chi_{l,k-1|k-1}, u_{k-1}) \tag{23}$$

The predicted state covariance is calculated as follows:

$$\begin{aligned}
\hat{x}^i_{k|k-1} &= \sum_{l=0}^{2n} W^m_l \chi_{l,k|k-1}\\
\hat{P}^i_{k|k-1} &= \sum_{l=0}^{2n} W^c_l (\chi_{l,k|k-1} - \hat{x}^i_{k|k-1})(\chi_{l,k|k-1} - \hat{x}^i_{k|k-1})^T
\end{aligned} \tag{24}$$

3) *Measurement update*. In the update step, the UKF up-dates the corrected state $\hat{x}^i_{k|k}$ and covariance $\hat{P}^i_{k|k}$ using measurement data from the in-vehicle sensors.

$$y_{l,k|k-1} = h_i(\chi_{l,k|k-1}, u_{k-1}) \tag{25a}$$

The predicted observation is computed by

$$\hat{y}^i_{k|k-1} = \sum_{l=0}^{2n} W^m_l y_{l,k|k-1} \tag{25b}$$

Since the observation noise is additive and independent, the innovation covariance is as

follows:

$$\hat{P}^i_{yy,k|k-1} = \sum_{l=0}^{2n} W_l^c (y_{l,k|k-1} - \hat{y}^i_{k|k-1})(y_{l,k|k-1} - \hat{y}^i_{k|k-1})^T + R \tag{26a}$$

The cross-correlation matrix is computed by

$$\hat{P}^i_{xy,k|k-1} = \sum_{l=0}^{2n} W_l^c (\chi_{l,k|k-1} - \hat{x}^i_{k|k-1})(y_{l,k|k-1} - \hat{y}^i_{k|k-1})^T \tag{26b}$$

Then, filter gain can be described as

$$K_k = \hat{P}^i_{xy,k|k-1} (\hat{P}^i_{yy,k|k-1})^{-1} \tag{27}$$

After the filter gain is obtained, the UKF updates the corrected state and covariance:

$$\begin{aligned} \hat{x}^i_{k|k} &= \hat{x}^i_{k|k-1} + K_k (y_k - \hat{y}^i_{k|k-1}) \\ \hat{P}^i_{k|k} &= \hat{P}^i_{k|k-1} - K_k \hat{P}^i_{yy,k|k-1} K_k^T \end{aligned} \tag{28}$$

3.3. Model probability update

Under the Gaussian assumption, the likelihood function of each mode and the model probability, respectively, can be updated by

$$\Lambda_{i,k} = \frac{\exp\left[-\frac{1}{2}(y_k - \hat{y}^i_{k|k-1})(\hat{P}^i_{yy,k|k-1})^{-1}(y_k - \hat{y}^i_{k|k-1})^T\right]}{\sqrt{2\pi S^i_k}} = \frac{\exp\left[-\frac{1}{2}(N^i_k)(S^i_k)^{-1}(N^i_k)^T\right]}{\sqrt{2\pi S^i_k}} \tag{29}$$

$$\mu_{i,k} = \frac{1}{c} \Lambda_{i,k} \bar{c}_i \tag{30a}$$

where N^i_k and S^i_k are the innovation and its covariance, respectively, and c is the normalization factor given by

$$c = \sum_{j=1}^{2} \Lambda_{i,k} \bar{c}_j \tag{30b}$$

3.4. Estimation fusion

Combining the results from their mode-matched filters that is based on the respective mode probabilities, the vehicle state estimation and its covariance can be obtained by using the Gaussian mixture equation. The vehicle state estimation and its covariance can be written as

$$\hat{x}_{k|k} = \sum_{i=1}^{2} \mu_{i,k} \hat{x}^i_{k|k} \tag{31}$$

$$\hat{P}_{k|k} = \sum_{i=1}^{2} \mu_{i,k} \left[\hat{P}^i_{k|k} + (\hat{x}^i_{k|k} - \hat{x}_{k|k})(\hat{x}^i_{k|k} - \hat{x}_{k|k})^T\right] \tag{32}$$

The mode probability $\mu_{i,k}$ is a weighting of the interaction and the combination of state estimation, which is very important for improving the estimation accuracy of vehicle state.

4. Simulation and analysis

4.1. Simulate conditions

CarSim is a widely used dynamic software that can simulate and analyze the dynamic handling behavior of different vehicles under diversiform driving conditions. It incorporates a 27-degree-of-freedom vehicle model, which is equipped with nonlinear tire models and virtual sensors as a standard feature. According to the parameters of the experimental electric vehicles in our laboratory, the simulation vehicle model was obtained using CarSim, and then utilizing CarSim and co-simulation between CarSim and Simulink, the numerical simulation of double-lane change (DLC) maneuvers is implemented to verify and evaluate the accuracy and performance of the proposed IMM estimator (the IMM-UKF and the IMM-EKF) for lateral tire–road forces and vehicle sideslip angle.

Fig. 7 presents the trajectory, longitudinal and lateral accelerations, and steering angle during DLC test. The acceleration diagram shows that the vehicle undergoes large lateral acceleration (absolute value up to 0.55 g), which means operated behavior of the vehicle dynamic in an extreme driving situation. The friction coefficient of the high-μ surface is set to be 0.9 in the simulation.

4.2. Validation of IMM-UKF estimator

The simulation results including the estimated lateral tire forces, the estimated longitudinal tire forces and the vehicle sideslip angle at the CG are shown in Figs.8–10. As can be seen from Figs.8–10, the estimated tire forces and the vehicle sideslip angle at the CG are close to the actual value, the IMM-UKF estimator shows high accuracy. Some small differences can be observed, which probably neglect the effect of the suspension kinematics and the camber angles for lateral forces component. As shown in Fig. 8, during the time intervals(4–5.5 s and 7.5–9 s), the estimated lateral tire forces of the right-hand side (Fig. 8(b) and (d)) are larger than that of the left-hand side (Fig. 8(a)), while the estimated lateral tire forces of the right-hand side are smaller than that of the left-hand side during the time interval (7.5–9 s). The phenomenon can be clearly explained due to the lateral load transfer that leads to the different lateral tire forces between the right-hand side and the left-hand side tires during cornering (Fig. 11). As shown in Fig. 4, lateral force increases as normal force increases in fact. The similar phenomenon can be found in Fig. 9. Initially, the estimated longitudinal force on the rear right tire is larger than that on the front right tire, which can be also explained by longitudinal load transfer during acceleration process.

According to (3)–(11), the tire slip angle and the normal force at each tire can be calculate from estimated states and measurement. Fig. 10 presents the variations of the normal forces on the front and rear tires. Fig. 12 shows how tire sideslip angles change during the double-lane change maneuvers.

Fig. 13 describes the model probability that represents the suitability of the vehicle model for the relevant driving conditions, which was calculated by utilizing the IMM-UKF estimator. As can be seen in Fig. 13, under normal driving conditions, the model probability of the linear tire model based NVDM and the nonlinear Dugoff tire model based NVDM were nearly equal

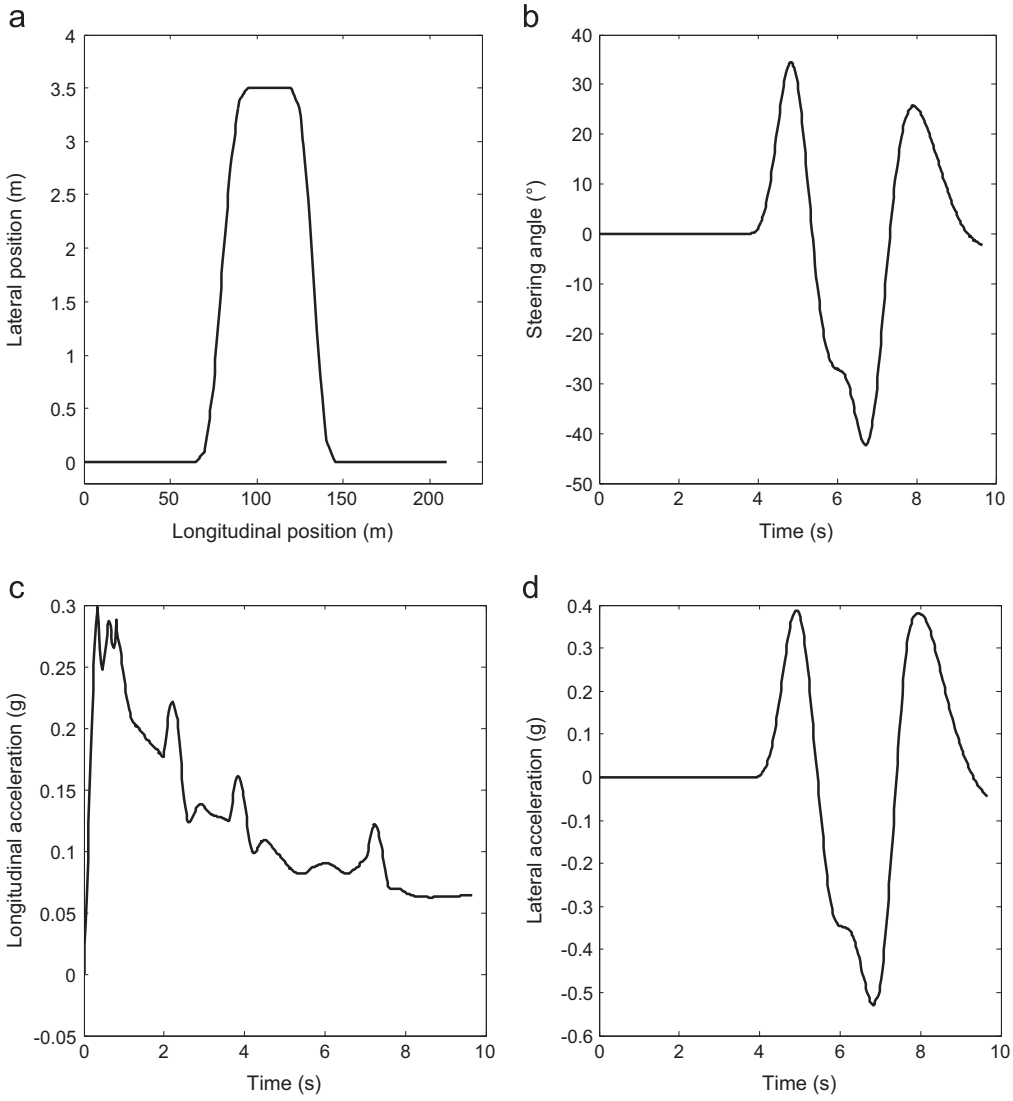

Fig. 7. Simulate conditions: (a) vehicle trajectory, (b) steering angle, (c) longitudinal acceleration and (d) lateral acceleration for the double-lane change maneuvers.

(about 0.5). This means that the tire operates in this linear region, the linear tire model based NVDM and the nonlinear Dugoff tire model based NVDM are both appropriate. However, during the time intervals (4.8–5.2 s, 5.9–7.2 s, and 7.7–8.3 s), the model probability of the nonlinear Dugoff tire model based NVDM (about 0.95) was much greater than that of the linear tire model based NVDM(about 0.05). This indicates that the tire operates in this nonlinear region, only the nonlinear Dugoff tire model based NVDM is suitable because it considers nonlinearity of the tire.

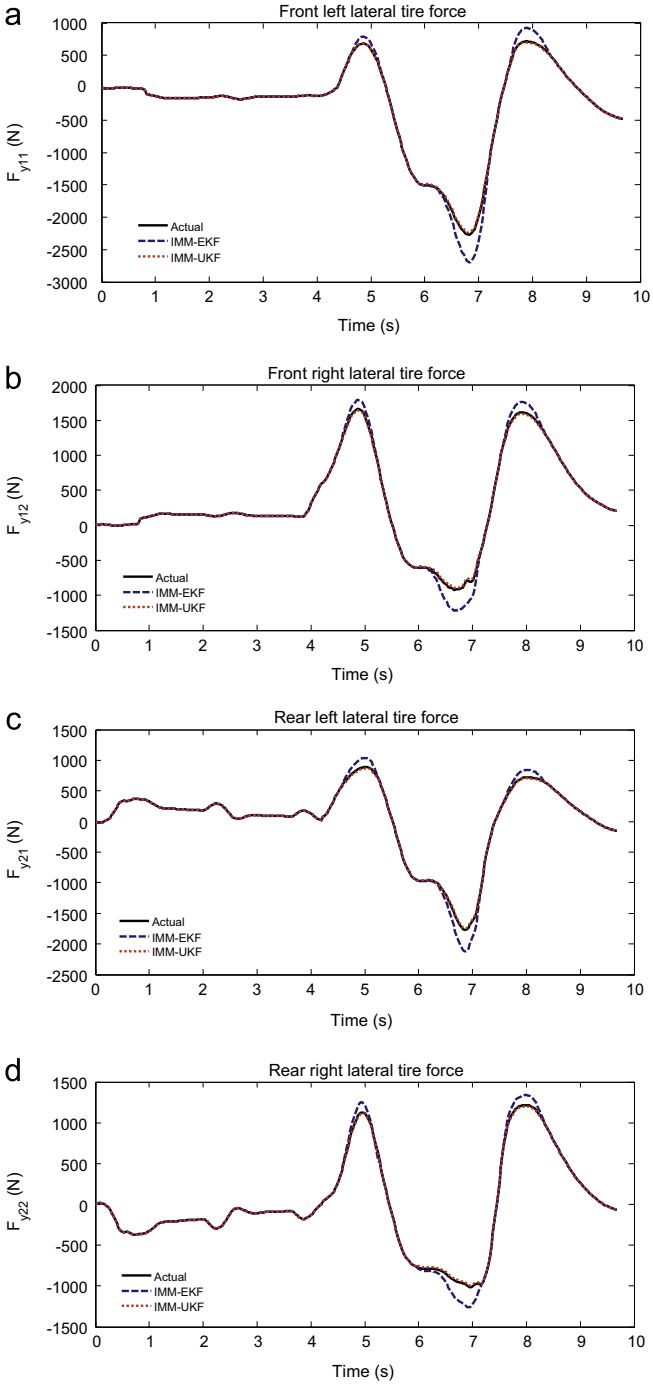

Fig. 8. Estimation for lateral tire–road forces on the front and rear tires.

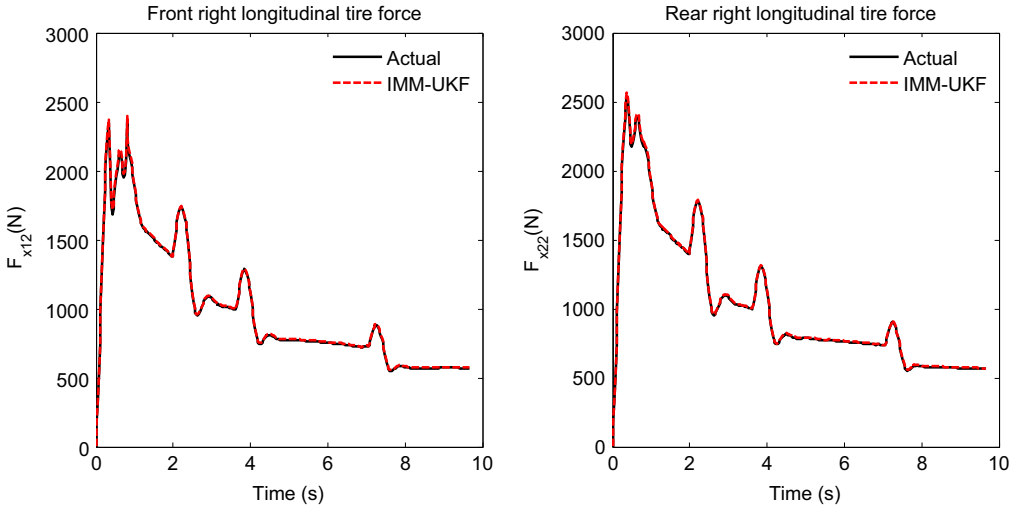

Fig. 9. Estimation for longitudinal forces on the front right and rear right tires.

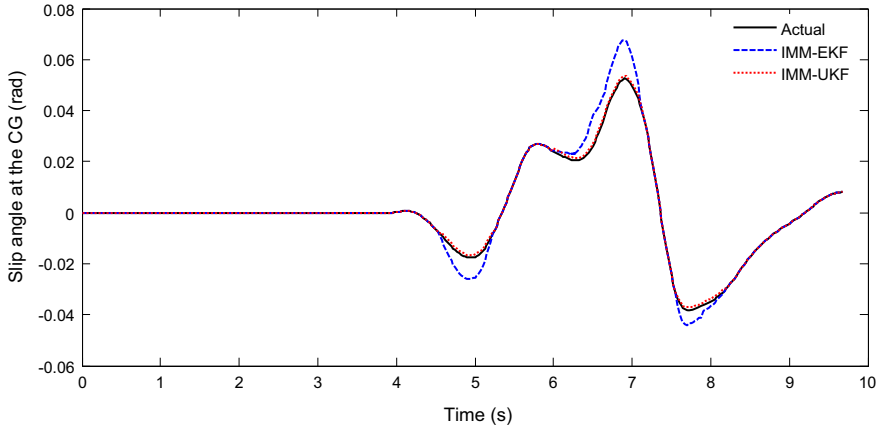

Fig. 10. Estimation of the vehicle sideslip angle at the CG.

4.3. Comparison between IMM-UKF estimator and IMM-EKF estimator

According to the numerical simulation results, two estimators based on the IMM-UKF and the IMM-EKF are compared. As shown in Fig. 8 and Fig. 10, the initial action of the IMM-EKF is similar to IMM-UKF. However, during the time intervals (4.8–5.2 s, 5.9–7.2 s, and 7.7–8.3 s), when heavy demands are made on the vehicle, large errors can be observed in the estimated lateral tire forces and the vehicle sideslip angle at the CG for the IMM-EKF. This phenomenon is due to the strong nonlinearities of tires nonlinear behavior and the vehicle nonlinear dynamics. In fact, as can be seen from Fig. 7(c) and (d) to Fig. 12, the vehicle undergoes high accelerations (absolute value up to 0.55 g), high tire sideslip angles (maximal value up to 6°) occur and the tire

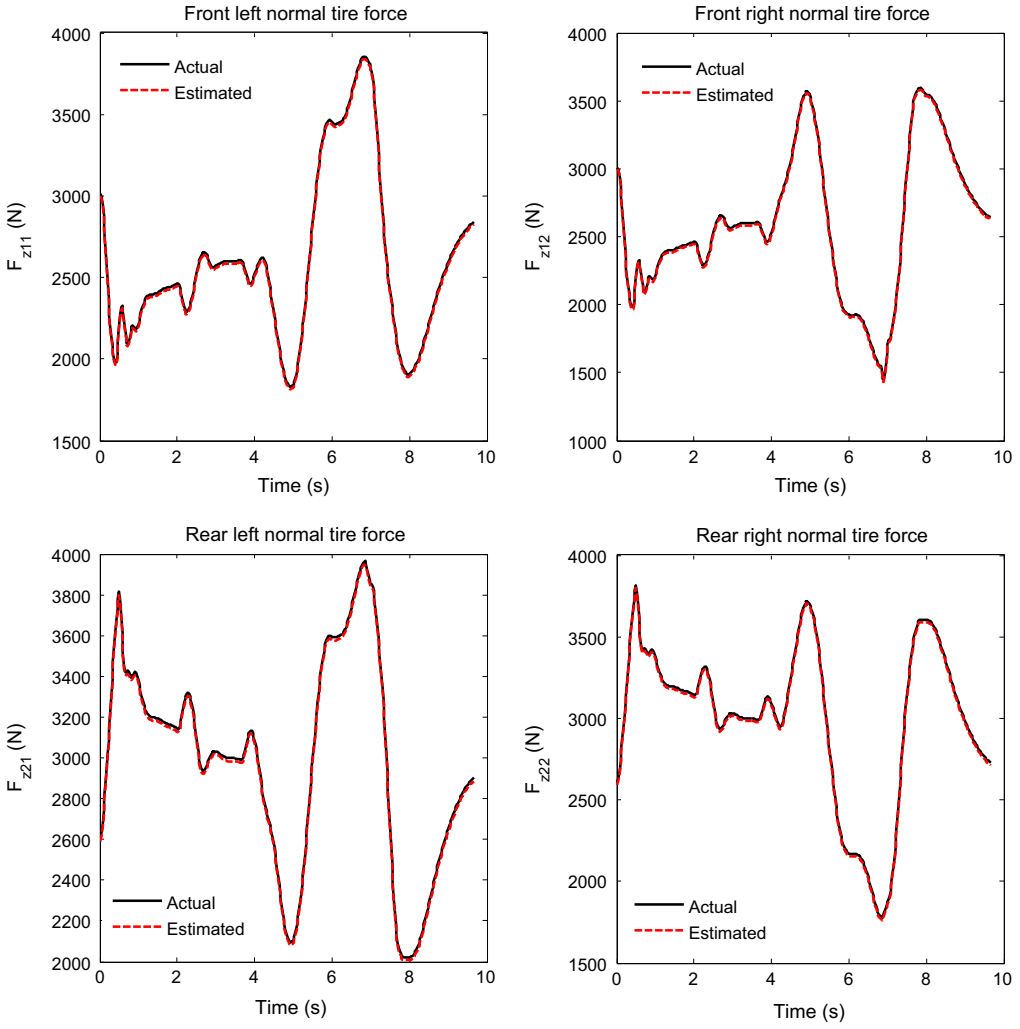

Fig. 11. Normal forces on the front and rear tires.

operates in the nonlinear region(Fig. 4). Then the vehicle's dynamic based on the tire becomes highly nonlinear. The large error means that linearization errors of the IMM-EKF are significant since the IMM-EKF uses Jacobian matrices to linearly approximate nonlinear system with first-order linearization. The IMM-UKF estimator shows its ability to overcome this difficulty, hence the performance of the proposed IMM-UKF is far better than that the IMM-EKF.

5. Conclusion

This paper has presented novel estimation methods to accurately estimate the vehicle sideslip angle and the lateral tire–road forces using in-vehicle sensors. Two estimators based on the IMM-UKF and the IMM-EKF are investigated and compared through simulations. The proposed IMM-based estimator combines the UKF/EKF estimates from two kinds of different vehicle–

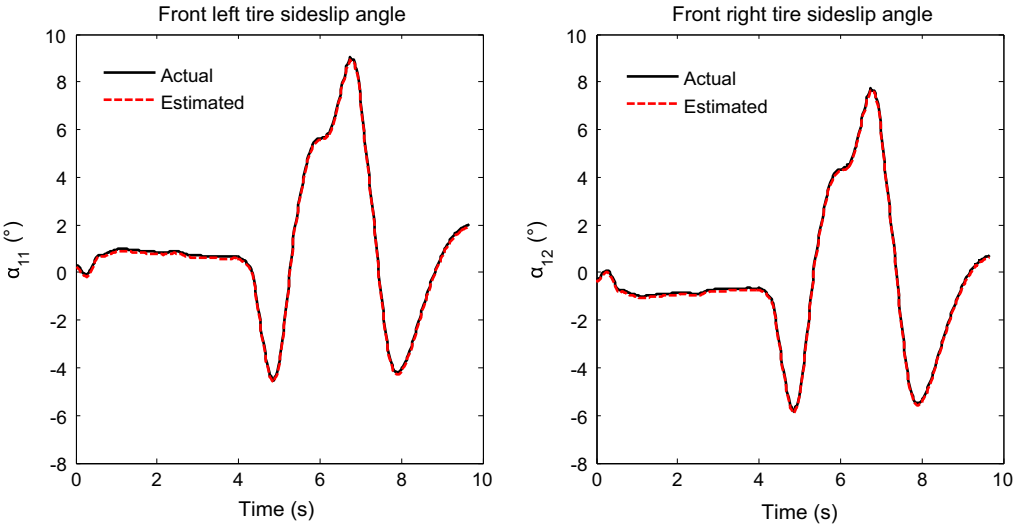

Fig. 12. The tire sideslip angles on front left and front right tires.

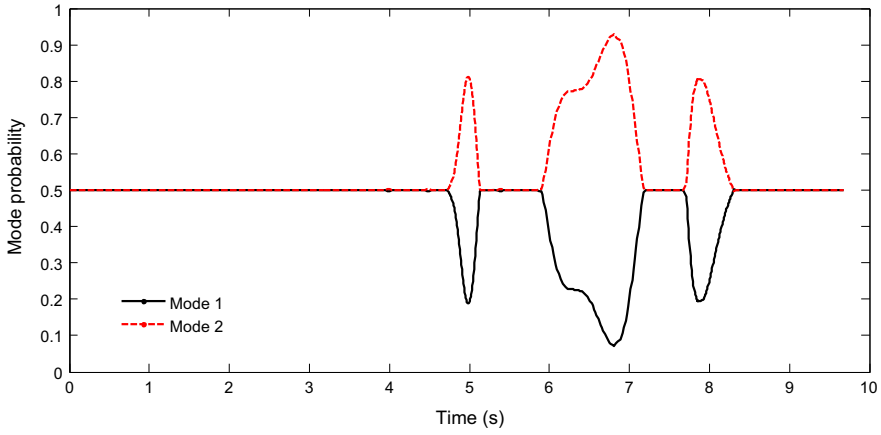

Fig. 13. Mode probability for the double-lane change maneuvers.

road system models to adapt to variable driving conditions. Under normal driving conditions, the suitability of the linear tire model based NVDM and the nonlinear Dugoff tire model based NVDM were nearly equal. Under extreme driving maneuvers, the nonlinear Dugoff tire model based NVDM model is more suitable compared with the linear tire model based NVDM. It is found from the results that the proposed IMM-UKF estimator provides more accurate and reliable estimates as compared to IMM-EKF estimator under variable driving conditions.

In future works, the vehicle–road system model will be improved to adapt to various road conditions (especially for the variable road friction coefficient,), and the real vehicle test and a hardware-in-the-loop simulation will be implemented to further validate the effectiveness of the proposed IMM-based estimator. Moreover, advanced vehicle control systems based on the proposed estimators will be researched.

Acknowledgment

The paper is supported by National Natural Science Foundation of China (No. 51105074), Foundation of State Key Laboratory of Mechanical Transmission (SKLMT-KFKT-201206) and Foundation of State Key Laboratory of Automotive Safety and Energy (KF14192).

References

[1] J Wang, R.G. Longoria, Coordinated and reconfigurable vehicle dynamics control, IEEE Trans. Control Syst. Technol. 17 (3) (2009) 723–732.
[2] R. Wang, J. Wang, Fault-tolerant control with active fault diagnosis for four-wheel independently-driven electric ground vehicles, IEEE Trans. Veh. Technol. 60 (9) (2011) 4276–4287.
[3] H. Zhang, Y. Shi, A.S. Mehr, Robust static output feedback control and remote PID design for networked motor systems, IEEE Trans. Ind. Electron. 58 (12) (2011) 5396–5405.
[4] J. Yamakawa, A. Kojimaa, K. Watanabe, A method of torque control for independent wheel drive vehicles on rough terrain, J. Terramech. 44 (5) (2007) 371–381.
[5] Z. Shuai, H. Zhang, J. Wang, J. Li, M. Ouyang, Combined AFS and DYC control of four-wheel-independent-drive electric vehicles over CAN network with time-varying delays, IEEE Trans. Veh. Technol. 63 (2) (2014) 591–602.
[6] R. Tchamna, I. Youn, Yaw rate and side-slip control considering vehicle longitudinal dynamics, Int. J. Automot. Technol. 14 (1) (2013) 53–60.
[7] M.C. Best, T.J. Gordon, P.J. Dixon, An extended adaptive Kalman filter for real-time state estimation of vehicle handling dynamics, Veh. Syst. Dyn. 34 (1) (2000) 57–75.
[8] G Baffet, A Charara, D Lechner, D Thomas, Experimental evaluation of observers for tire-road forces, sideslip angle and wheel cornering stiffness, Veh. Syst. Dyn. 46 (6) (2008) 501–520.
[9] G. Cong, L. Mostefai, M. Denai, Y. Hori, Direct yaw-moment control of an in-wheel-motored electric vehicle based on body slip angle fuzzy observer, IEEE Trans. Ind. Electron. 56 (5) (2009) 1411–1419.
[10] M. Doumiati, A.C. Victorino, A. Charara, D. Lechner, Onboard real-time estimation of vehicle lateral tire-road forces and sideslip angle, IEEE/ASME Trans. Mechatron. 16 (4) (2011) 601–614.
[11] J. Dakhlallah, N. Glaser, S. Mammar, Y. Sebsadji, Tire-road forces estimation using extended Kalman filter and sideslip angle evaluation, in: Proceedings of the American Control Conference, Seattle, WA, June 2008, pp. 4597–4602.
[12] X. Gao, Z. Yu, J. Neubeck, J. Wiedemann, Sideslip angle estimation based o n input-output linearisation with tire-road friction adaptation, Veh. Syst. Dyn. 48 (2) (2010) 217–234.
[13] S. You, J. Hahn, H. Lee, New adaptive approaches to real-time estimation o f vehicle sideslip angle, Control Eng. Pract. 17 (12) (2009) 1367–1379.
[14] D. Piyabongkarn, R. Rajamani, J. Grogg, J. Lew, Development and experimental evaluation o f a slip angle estimator for vehicle stability control, IEEE Trans. Control Syst. Technol. 17 (1) (2009) 78–88.
[15] F. Chelli, E. Sabbioni, M. Pesce, S. Melzi, A methodology for vehicle sideslip angle identification: comparison with experimental data, Veh. Syst. Dyn. 45 (6) (2007) 549–563.
[16] R. Wang, J. Wang, Tire–road friction coefficient and tire cornering stiffness estimation based on longitudinal tire force difference generation, Control Eng. Pract. 21 (1) (2012) 65–75.
[17] L.R. Ray, Nonlinear tire force estimation and road friction identification: simulation and experiments, Automatica 33 (10) (1997) 1819–1833.
[18] K. Nam, H. Fujimoto, Estimation of sideslip and roll angles of electric vehicles using lateral tire force sensors through RLS and Kalman filter approaches, IEEE Trans. Veh. Technol. 61 (5) (2012) (1792–1785).
[19] J. Ryu, J.C. Gerdes, Integrating inertial sensors with GPS for vehicle dynamics control, J. Dyn. Syst., Meas., Control 126 (2) (2004) 243–254.
[20] R. Daily, D.M. Bevly, The use of GPS for vehicle stability control systems, IEEE Trans. Ind. Electron. 51 (2) (2004) 270–277.
[21] D.M. Bevly, J. Ryu, J.C. Gerdes, Integrating INS sensors with GPS measurements for continuous estimation of vehicle sideslip, roll, and tire cornering stiffness, IEEE Trans. Intell. Transp. Syst. 7 (4) (2006) 483–493.
[22] S. Rezaei, R. Sengupta, Kalman filter-based integration of DGPS and vehicle sensors for localization, IEEE Trans. Control Syst. Technol. 15 (6) (2007) 1080–1088.

[23] G Yin, N Chen, P. Li, Improving handling stability performance of four-wheel steering vehicle via μ-synthesis robust control, IEEE Trans. Veh. Technol. 56 (5) (2007) 2432–2438.
[24] J. Wang, L. Alexander, R Rajamani, Friction estimation on highway vehicles using longitudinal measurements, ASME Trans. J. Dyn. Syst. Meas. Control 126 (2) (2004) 265–275.
[25] J. Kim, Effect of vehicle model on the estimation of lateral vehicle dynamics, Int. J. Auto. Tech-kor. 11 (3) (2010) 331–337.
[26] H. Zhang, X. Zhang, J. Wang, Robust gain-scheduling energy-to-peak control of vehicle lateral dynamics stabilisation, Veh. Syst. Dyn. 52 (3) (2014) 309–340.
[27] M. Dawood, C. Cappelle, M.E. El Najjar, M. Khalil, D. Pomorski, Vehicle geo-localization based on IMM-UKF data fusion using a GPS receiver, a video camera and a 3D city model, in: Proceedings of the IEEE Intelligent Vehicles Symposium (IV),2011, pp. 510–515.
[28] E. Mazor, A. Averbuch, Y. Bar-Shalom, J. Dayan, Interacting multiple model methods in target tracking: a survey, IEEE Trans. Aerosp. Electron. Syst. 34 (1) (1998) 103–123.
[29] J.F. Liao, B.S. Chen, Robust mobile location estimator with NLOS mitigation using interacting multiple model algorithm, IEEE Trans. Wireless Commun. 5 (11) (2006) 3002–3006.
[30] J. Dugoff, P. Fanches, L. Segel, An analysis of tire properties and their influence on vehicle dynamic performance, SAE Paper 700377, 1970.
[31] S.L. Koo, H.S. Tan, Tire dynamic deflection and its impact on vehicle longitudinal dynamics and control, IEEE/ASME Trans. Mechatron. 12 (6) (2007) 623–631.
[32] H. Zhang, Y. Shi, J. Wang, Observer-based tracking controller design for networked predictive control systems with uncertain Markov delays, Int. J. Control 86 (10) (2013) 1824–1836.
[33] K. Jo, K. Chu, M Sunwoo, Interacting multiple model filter-based sensor fusion of GPS with in-vehicle sensors for real-time vehicle positioning, IEEE Trans. Intell. Transp. Syst. 13 (1) (2012) 329–343.
[34] S.S. Blackman, R. Popoli, Design and Analysis of Modern Tracking Systems, Artech House, Noorwood, MA, 1999.
[35] H. Zhang, Y. Shi, J. Wang, On energy-to-peak filtering for nonuniformly sampled nonlinear systems: a Markovian jump system approach, IEEE Trans. Fuzzy Syst. 22 (1) (2014) 212–222.